

Substituted Metal Carbonyls. 27.¹ Synthesis, Structures, and Metal–Metal Bonding of a Ferrocenylphosphine *exo*-Bridged Cluster with Two Heterometallic Triangles, $[\text{AuMn}_2(\text{CO})_8(\mu\text{-PPh}_2)]_2(\mu\text{-dppf})$, and a Twisted-Bowtie Cluster, $\text{PPN}^+[\text{Au}\{\text{Mn}_2(\text{CO})_8(\mu\text{-PPh}_2)\}_2]^-$ (dppf = 1,1'-Bis(diphenylphosphino)ferrocene)

Pauline M. N. Low, Agnes L. Tan,[†] and T. S. Andy Hor*

Department of Chemistry, Faculty of Science, National University of Singapore, Kent Ridge, Singapore 119260

Yuh-Sheng Wen and Ling-Kang Liu*

Institute of Chemistry, Academia Sinica, Taipei 11529, Taiwan, ROC

Received October 10, 1995[⊗]

Redox condensation of $\text{PPN}[\text{Mn}_2(\text{CO})_8(\mu\text{-PPh}_2)]$ (**1**; $\text{PPN} = \text{N}(\text{PPh}_3)_2$) with $\text{Au}_2\text{Cl}_2(\mu\text{-P-P})$ ($\text{P-P} = (\text{C}_5\text{H}_4\text{PPh}_2)_2\text{Fe}$ (dppf), $\text{Ph}_2\text{PC}_2\text{H}_4\text{PPh}_2$ (dppe)) gives two hexanuclear Au–Mn clusters $[\text{AuMn}_2(\text{CO})_8(\mu\text{-PPh}_2)]_2(\mu\text{-P-P})$ ($\text{P-P} = \text{dppf}$, (**2**), dppe (**4**)), both of which contain a diphosphine bridging two Mn_2Au triangles. Complex **2** is formed via an intermediate, $\text{AuCl}(\mu\text{-dppf})[\text{AuMn}_2(\text{CO})_8(\mu\text{-PPh}_2)]$, (**3**), which was isolated. Bridge cleavage of **2** occurs at the reflux with PPh_3 and room temperature with $\text{P}(\text{OEt})_3$ to give the triangular clusters $[(\text{PR}_3)\text{-AuMn}_2(\text{CO})_8(\mu\text{-PPh}_2)]$ ($\text{R} = \text{Ph}$ (**5**), OEt (**6**)), respectively. The latter exchange of dppf with $\text{P}(\text{OEt})_3$ is reversible in solution. Condensation of **1** with $\text{AuCl}(\text{SMe}_2)$ gives an anionic pentanuclear cluster, $\text{PPN}[\text{Au}\{\text{Mn}_2(\text{CO})_8(\mu\text{-PPh}_2)\}_2]$ (**7**). Complexes **2** and **7** were structurally characterized by single-crystal X-ray diffractometry. Complex **2**, which is centrosymmetric with Fe in dppf at a crystallographic inversion center, consists of a ferrocenylphosphine bridging two heterometallic triangles ($\text{Au-Mn} = 2.660(1)$ and $2.776(1)$ Å; $\text{Mn-Mn} = 3.049(2)$ Å). Complex **7** is made up of two planar AuMn_2P metallacycles fused at Au at an angle of $85.50(4)^\circ$. With crystallographic C_2 symmetry, a twisted-bowtie skeleton resulted with gold at its center. Both Au-Mn (mean $2.806(1)$ Å) and $(\text{PPh}_2\text{-bridged}) \text{Mn-Mn}$ ($3.105(2)$ Å) lengths are significantly longer than those in **2**. The Mn-Mn bond of **2** is also significantly longer than that of **1**. Fenske–Hall MO calculations on **1**, **2**, and **7** together with $\text{Mn}_2(\text{CO})_8(\mu\text{-H})(\mu\text{-PPh}_2)$ (**8**) and $(\text{PPhMe}_2)\text{AuMn}_2(\text{CO})_8(\text{PPh}_2)$ (**9**) indicate that aside from **1**, all the complexes, including **2** and **7**, give a negative overlap population in the Mn-Mn interactions. The Mn-Mn distance appears to be determined by the strength of the AuMn_2 interaction and/or the size of H compared to Au. The weaker Mn-Mn and Au-Mn interactions in **7** (as compared to those in **2** and **9**, respectively) are likely to be caused by the absence of Au orbital reinforcement in the direction of the Mn_2 moiety as a consequence of symmetry.

Introduction

Heterometallic gold clusters have attracted attention because of their unusual bonding and structural properties.² The catalytic enhancement of gold in some of these carbonyl clusters³ provides an added impetus for research in this area. Many of these species are synthesized by nucleophilic attack of metal carbonyl anions on $\text{AuCl}(\text{PR}_3)^{4-6}$ or condensation of metal carbonyl hydrides with $\text{AuMe}(\text{PR}_3)$ or $\text{AuCl}(\text{PR}_3)$, eliminating CH_4 or HCl .^{7,8} The isolobal relationship of $[\text{AuPR}_3]$ with $[\text{H}]$ also enables the designed syntheses of many

of these clusters. One notable example is $\text{Os}_3(\text{CO})_{10}(\mu\text{-AuPPh}_3)(\mu\text{-H})$,^{6a} which represents an isolobal replace-

(2) Mingos, D. M. P.; Wales, D. J. *Introduction to Cluster Chemistry*; Prentice-Hall: Englewood Cliffs, NJ, 1990; Chapter 4, p 154. Mingos, D. M. P.; Watson, M. J. *Adv. Inorg. Chem.* **1992**, *39*, 327. Bott, S. G.; Mingos, D. M. P.; Watson, M. J. *J. Chem. Soc., Chem. Commun.* **1989**, 1192. Teo, B. K.; Keating, K. *J. Am. Chem. Soc.* **1984**, *106*, 2224. Teo, B. K.; Zhang, H.; Shi, X. *J. Am. Chem. Soc.* **1993**, *115*, 8489. Teo, B. K.; Shi, X.; Zhang, H. *Inorg. Chem.* **1993**, *32*, 3987. Teo, B. K.; Zhang, H.; Shi, X. *Inorg. Chem.* **1994**, *33*, 4086. Contel, M.; Jimenez, J.; Jones, P. G.; Laguna, A.; Laguna, M. *J. Chem. Soc., Dalton Trans.* **1994**, 2515. Kappen, T. G. M. M.; Schlebos, P. P. J.; Bour, J. J.; Bosman, W. P.; Smits, J. M. M.; Beurskens, P. T.; Steggerda, J. *J. Inorg. Chem.* **1994**, *33*, 754. Johnson, A. J. W.; Spencer, B.; Dahl, L. F. *Inorg. Chim. Acta* **1994**, *227*, 269. Gould, R. A. T.; Craighead, K. L.; Wiley, J. S.; Pignolet, L. H. *Inorg. Chem.* **1995**, *34*, 2902.

(3) Evans, J.; Gao, J. *J. Chem. Soc., Chem. Commun.* **1985**, 39. Braunstein, P.; Rose, J. *Gold Bull.* **1985**, *18*, 17.

(4) Haines, R. J.; Nyholm, R. S.; Stiddard, M. H. B. *J. Chem. Soc. A* **1968**, 46. Green, M.; Orpen, A. G.; Salter, I. D.; Stone, F. G. A. *J. Chem. Soc., Dalton Trans.* **1984**, 2897.

(5) (a) Coffey, C. E.; Lewis, J.; Nyholm, R. S. *J. Chem. Soc.* **1964**, 1741. (b) Kasenally, A. S.; Lewis, J.; Manning, A. R.; Miller, J. R.; Nyholm, R. S.; Stiddard, M. H. B. *J. Chem. Soc.* **1965**, 3407.

* To whom correspondence should be addressed.

[†] Computational Science Programme, National University of Singapore.

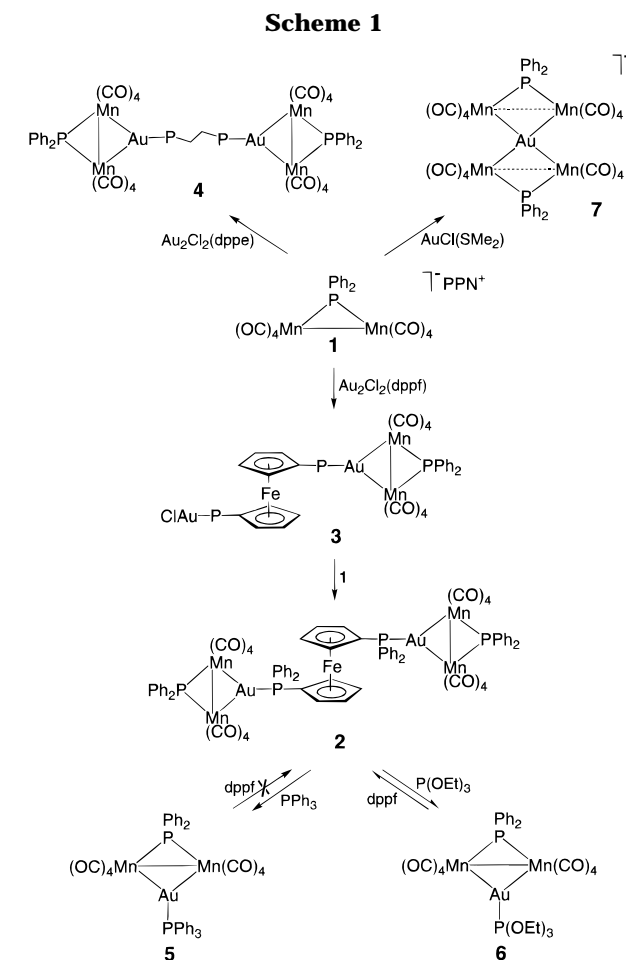
[⊗] Abstract published in *Advance ACS Abstracts*, May 1, 1996.

(1) Part 26: Low, P. M. N.; Yong, Y. L.; Hor, T. S. A.; Lam, S.-L.; Chan, K. W.; Wu, C.; Au-Yeung, S. C. F.; Wen, Y.-S.; Liu, L.-K. *Organometallics* **1996**, *15*, 1369.

ment of hydride in $\text{Os}_3(\text{CO})_{18}(\mu\text{-H})_2^9$ by an $[\text{Au}(\text{PPh}_3)]$ fragment. As a result, pioneering work by Nyholm *et al.* in 1964 in which various simple bimetallic complexes were made by coupling metal carbonylate anions (e.g. $[\text{Mn}(\text{CO})_5]^-$ and $[\text{Co}(\text{CO})_4]^-$) with $\text{AuCl}(\text{PPh}_3)^{5a}$ can simply be rationalized by the isolobal principle. Our recent isolation of the Au–M-bonded (M = Mn, Re) complexes $[\text{AuM}(\text{CO})_5]_2(\mu\text{-dppf})^{10}$ proved that this synthetic methodology can be extended to $\text{Au}_2\text{Cl}_2(\mu\text{-dppf})$. In this case, the complex behaves as a useful Au(I) analogue of a dibasic acid. The synthetic value of this “acid” is that, since the “protons” are linked by an electroactive ferrocenyl group, upon “protonation” of two di-, tri-, or polynuclear metal carbonylates, one can accomplish a one-step access to ferrocenyl-bridged clusters¹¹ which are molecular analogues of electroactive materials.¹² This novel yet simple approach to ferrocenylphosphine *exo*-bridged heterometallic metal triangles is described in this paper. The precursor PPN- $[\text{Mn}_2(\text{CO})_8(\mu\text{-PPh}_2)]$ is chosen on the basis of our experience with $[\text{AuMn}(\text{CO})_5]_2(\mu\text{-dppf})$ and the well-known auration of this anion with $[\text{Au}(\text{PR}_3)]$ fragments across the Mn–Mn bond without Mn–Mn fragmentation.^{13,14} A similar approach in the literature using a mononuclear carbonylate resulted in the isolation of simple bimetallics such as $(\text{OC})_5\text{MnAu}(\text{PR}_3)^5$ (R = Ph, PhO, *p*-MeO-C₆H₄) or closed clusters such as $[(\text{Ph}_3\text{PAu})_4\text{Mn}(\text{CO})_4]\text{BF}_4^{15}$ and $(\text{Ph}_3\text{PAu})_3\text{Mn}(\text{CO})_3^{15,16}$. We shall also describe the use of a labile Au(I) complex such as $\text{AuCl}(\text{SMe}_2)$ to synthesize a heterometallic compound which is similar but which has an open structure. The effects of different isolobal fragments, *viz.* $[\text{Au}_2(\text{dppf})]$, $[\text{Au}(\text{PR}_3)]$, and $[\text{H}]$, on the strength of the Mn–Mn bonds in relation to that of the Au–Mn bonds in the heterometallic complexes synthesized will also be examined with the aid of theoretical calculations.

Results and Discussion

When an equimolar amount of $[\text{Au}_2(\mu\text{-dppf})](\text{BF}_4)_2$ (generated *in situ* from $\text{Au}_2\text{Cl}_2(\mu\text{-dppf})$ and AgBF_4 (1.0:2.6)) was added to **1** (from reduction of $[\text{Mn}_2(\text{CO})_8(\mu\text{-PPh}_2)]^{17}$ by NaBH_4), redox condensation resulted and $[\text{AuMn}_2(\text{CO})_8(\mu\text{-PPh}_2)]_2(\mu\text{-dppf})$ (**2**) and $\text{AuCl}(\mu\text{-dppf})[\text{AuMn}_2(\text{CO})_8(\mu\text{-PPh}_2)]$ (**3**) were isolated in 51% and 13% yields, respectively. If AgBF_4 was omitted and the addition of the two substrates reversed, *viz.* by adding PPN $[\text{Mn}_2(\text{CO})_8(\mu\text{-PPh}_2)]$ to $\text{Au}_2\text{Cl}_2(\mu\text{-dppf})$, the yield of **2** remained at 50% but that of **3** increased to 20%. When **1** was added to $[\text{Au}_2(\mu\text{-dppf})](\text{BF}_4)_2$ in a 2:1 mole ratio, the yield of **2** increased further to 65% and that of **3** was negligible. These observations suggested that **3** is formed as a result of incomplete substitution of Cl^- in $\text{Au}_2\text{Cl}_2(\mu\text{-dppf})$ by the anionic **1** (Scheme 1). Both **2** and **3** have been fully characterized by IR and ¹H and ³¹P NMR spectroscopy. The structure of **2** has also been established by X-ray crystallography.



The IR bands in the carbonyl region of **2** and **3** are similar to those of $(\text{PPhR}_2)\text{AuMn}_2(\text{CO})_8(\mu\text{-PPh}_2)$ (R = Ph,¹³ Me¹⁴) and $\text{Mn}_2(\text{CO})_8(\mu\text{-PPh}_2)(\mu\text{-H})$.¹⁷ This suggests the maintenance of a $[\text{Mn}_2(\text{CO})_8]$ moiety and the similar coordination behavior of the $[\text{Au}_2(\text{dppf})]$ as compared to

The ³¹P NMR spectrum of **2** shows a sharp singlet at δ 58.02 ppm attributed to the phosphine attached to the gold atom and a very low-field resonance (δ 212.31 ppm) characteristic of the bridging phosphido group. The latter is broadened by the neighboring ⁵⁵Mn quadrupolar nuclei. Similar features are found in **3** but with an additional resonance at δ 27.82 ppm, which is consistent with a pendant Au–P site (cf. $\text{Au}_2\text{Cl}_2(\mu\text{-dppf})$, δ 28.27 ppm).

The IR bands in the carbonyl region of **2** and **3** are similar to those of $(\text{PPhR}_2)\text{AuMn}_2(\text{CO})_8(\mu\text{-PPh}_2)$ (R = Ph,¹³ Me¹⁴) and $\text{Mn}_2(\text{CO})_8(\mu\text{-PPh}_2)(\mu\text{-H})$.¹⁷ This suggests the maintenance of a $[\text{Mn}_2(\text{CO})_8]$ moiety and the similar coordination behavior of the $[\text{Au}_2(\text{dppf})]$ as compared to

(6) (a) Johnson, B. F. G.; Kaner, D. A.; Lewis, J.; Raithby, P. R. *J. Organomet. Chem.* **1981**, *215*, C33. (b) Johnson, B. F. G.; Kaner, D. A.; Lewis, J.; Raithby, P. R.; Rosales, M. J. *J. Organomet. Chem.* **1982**, *231*, C59. (c) Johnson, B. F. G.; Lewis, J.; Nelson, W. J. H.; Raithby, P. R.; Vargas, M. D. *J. Chem. Soc., Chem. Commun.* **1983**, 608. (d) Briant, C. E.; Hall, K. P.; Mingos, D. M. P. *J. Chem. Soc., Chem. Commun.* **1983**, 843.

(7) Luke, M. A.; Mingos, D. M. P.; Sherman, D. J.; Wardle, R. W. *Transition Met. Chem.* **1987**, *12*, 37. Casalnuova, A. L.; Laska, T.; Nilsson, P. V.; Olofson, J.; Pignolet, L. H. *Inorg. Chem.* **1985**, *24*, 233.

(8) Green, M.; Mead, K. A.; Mills, R. M.; Salter, I. D.; Stone, F. G. A.; Woodward, P. *J. Chem. Soc., Chem. Commun.* **1982**, 51. Bateman, L. W.; Green, M.; Howard, J. A. K.; Mead, K. A.; Mills, R. M.; Salter, I. D.; Stone, F. G. A.; Woodward, P. *J. Chem. Soc., Chem. Commun.* **1982**, 773.

(9) Orpen, A. G.; Riera, A. V.; Bryan, E. G.; Pippard, D.; Sheldrick, G.; Rouse, K. D. *J. Chem. Soc., Chem. Commun.* **1978**, 723.

(10) Low, P. M. N.; Yan, Y. K.; Chan, H. S. O.; Hor, T. S. A. *J. Organomet. Chem.* **1993**, *454*, 205.

(11) Fang, Z.-G.; Wen, Y.-S.; Wong, R. K. L.; Ng, S.-C.; Liu, L.-K.; Hor, T. S. A. *J. Cluster Sci.* **1994**, *5*, 327.

(12) Togni, A. In *Ferrocenes*; Togni, A., Hayashi, T., Eds.; VCH: Weinheim, Germany, 1995; Chapter 8, p 433.

(13) Haupt, H.-J.; Heinekamp, C.; Flörke, U.; Jüptner, U. *Z. Anorg. Allg. Chem.* **1992**, *608*, 100.

(14) Iggo, J. A.; Mays, M. J.; Raithby, P. R.; Hendrick, K. *J. Chem. Soc., Dalton Trans.* **1984**, 633.

(15) Nicholson, B. K.; Bruce, M. I.; bin Shawkataly, O.; Tiekink, E. R. T. *J. Organomet. Chem.* **1992**, *440*, 411.

(16) Ellis, J. E.; Faltynek, R. A. *J. Chem. Soc., Chem. Commun.* **1975**, 966.

(17) Iggo, J. A.; Mays, M. J.; Raithby, P. R.; Hendrick, K. *J. Chem. Soc., Dalton Trans.* **1983**, 205.

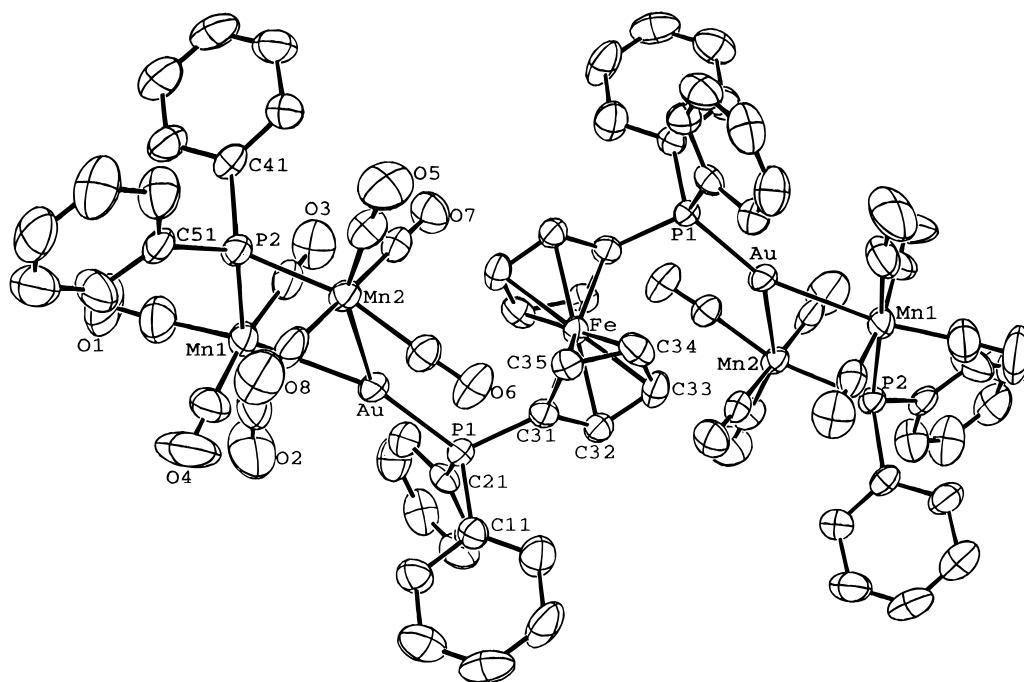


Figure 1. ORTEP drawing of the structure of $[\text{AuMn}_2(\text{CO})_8(\mu\text{-PPh}_2)_2(\mu\text{-dppf})]$ (**2**).

Table 1. Crystallographic Data for $[\text{AuMn}_2(\text{CO})_8(\mu\text{-PPh}_2)_2(\mu\text{-dppf})]$ (2**) and $\text{PPN}[\text{Au}\{\text{Mn}_2(\text{CO})_8(\mu\text{-PPh}_2)\}_2]$ (**7**)**

	2	7
chem formula	$\text{C}_{74}\text{H}_{48}\text{Au}_2\text{FeMn}_4\text{O}_{16}\text{P}_4$	$\text{C}_{76}\text{H}_{50}\text{AuMn}_4\text{NO}_{16}\text{P}_4$
fw	1987	1774
cryst syst	monoclinic	monoclinic
space group	$P2_1/c$	$C2/c$
<i>a</i> , Å	14.592(2)	24.332(6)
<i>b</i> , Å	14.675(2)	17.517(4)
<i>c</i> , Å	16.658(2)	17.245(6)
β , deg	91.46(1)	104.29(24)
<i>V</i> , Å ³	3565.9(8)	7123(3)
<i>Z</i>	2	4
<i>d</i> _{calcd} , g cm ⁻³	1.850	1.654
<i>T</i> , K	298	298
$\lambda(\text{Mo K}\alpha)$, Å	0.709 30	0.710 69
μ , mm ⁻¹	5.10	2.86
no. of obsd rflns	3462	3169
<i>R</i> ^a	0.030	0.031
<i>R</i> ^b	0.035	0.033

$$^a R = \sum ||F_o| - |F_c|| / \sum |F_o|. \quad ^b R' = (\sum w(|F_o| - |F_c|)^2 / \sum w|F_o|^2)^{1/2}.$$

two [H] or $[\text{Au}(\text{PR}_3)]$ fragments. The X-ray single-crystal diffraction study confirmed the solution findings and showed that with both gold atoms of $\text{Au}_2\text{Cl}_2(\text{dppf})$ inserted into the Mn–Mn bonds in two anions of **1**, complex **2** is a dimeric analogue of $(\text{PR}_3)\text{AuMn}_2(\text{CO})_8(\mu\text{-PPh}_2)$ ^{13,14} (Figure 1). It is centrosymmetric with the Fe atom at the center of inversion. The ferrocenyl C₅ rings are exactly staggered ($\tau = 180^\circ$) as a condition of this inversion. This staggered arrangement of the C₅ rings is often but not always found in many open-bridged dppf complexes.¹⁸ Complex **2** can thus be viewed as two heterometallic AuMn_2 triangles singly bridged by dppf. This concept of linked clusters has been described elsewhere in which ligands (“fillers”) are used to link two identical or different cluster fragments.¹⁹ Complex **2** is, however, the only example of heterometallic clusters which are joined similarly. Heteropolymetallic oligomers bridged by dppf have been

discussed by us recently.²⁰ An alternative view of **2** is that two Mn–Mn-bonded dimers are bridged by a heterometallic fragment, $[\text{Au}\text{-dppf}\text{-Au}]$. The phosphide bridge is symmetrically disposed ($\Delta(\text{Mn}\text{-P}) = 0.005(2)$ Å) but not the gold bridge ($\Delta(\text{Au}\text{-Mn}) = 0.116(1)$ Å). The asymmetric disposition of the latter is manifested in the uneven $\angle\text{Au}\text{-Mn}(1,2)\text{-Mn}(2,1)$ ($\Delta = 3.62(3)^\circ$) and $\angle\text{Au}\text{-Mn}(1,2)\text{-C}(1,5)$ ($\Delta = 6.5(3)^\circ$) angles.

In order to illustrate that this approach to form ligand-bridged cluster triangles is applicable to other diphosphines such as $\text{Ph}_2\text{P}(\text{CH}_2)_n\text{PPh}_2$, we have similarly obtained $[\text{AuMn}_2(\text{CO})_8(\mu\text{-PPh}_2)_2(\mu\text{-dippe})]$ (**4**) from $\text{Au}_2\text{Cl}_2(\mu\text{-dippe})$. The isolation of **4** may suggest that these clusters could tolerate bridges of different chain lengths.

In a study to examine the strength of the cluster bridge, a representative phosphine (PPh_3) or phosphite ($\text{P}(\text{OEt})_3$) was added in excess to complex **2**. Phosphine displacement readily occurs to give 2 equiv of $(\text{PR}_3)\text{-AuMn}_2(\text{CO})_8(\mu\text{-PPh}_2)$ ($\text{R} = \text{Ph}$ (**5**), $\text{P}(\text{OEt})_3$ (**6**)). The expected ease of bridge cleavage can be explained on the basis of steric and entropic grounds. The ability for the incoming PR_3 to undergo associative displacement on a 14-electron gold center also explains the kinetic facility. The observed displacement of dppf is in contrast to the dissociation of $[\text{Au}(\text{PET}_3)]^+$ (identified as $[\text{Au}(\text{PET}_3)_2]^+$) from $(\text{PET}_3)\text{AuMn}_2(\text{CO})_8(\mu\text{-PPh}_2)$ in a similar reaction of the latter with PET_3 .¹⁴

The isolation of a pure sample of **6** from **2** was plagued by the ease of phosphite dissociation and the reentry of adventitious dppf. This reversibility demonstrates a fine balance among the entropy factors, the kinetic lability of $\text{P}(\text{OEt})_3$, and the preference of gold for a

(18) Gan, K.-S.; Hor, T. S. A. In *Ferrocenes*; Togni, A., Hayashi, T., Eds.; VCH: Weinheim, Germany, 1995; Chapter 1, p 3

(19) Cullen, W. R.; Rettig, S. J.; Zheng, T. *Organometallics* **1992**, *11*, 928. Le Grand, J.-L.; Lindsell, W. E.; McCullough, K. J.; McIntosh, C. H.; Meiklejohn, A. G. *J. Chem. Soc., Dalton Trans.* **1992**, 1089. Tunik, S. P.; Osipov, M. V.; Nikolskiy, A. B. *J. Organomet. Chem.* **1992**, *426*, 105. Sappa, E. *J. Organomet. Chem.* **1988**, *352*, 327.

(20) Phang, L.-T.; Gan, K.-S.; Lee, H. K.; Hor, T. S. A. *J. Chem. Soc., Dalton Trans.* **1993**, 2697.

Table 2. Selected Bond Lengths (Å) and Angles (deg)

(a) [AuMn ₂ (CO) ₈ (μ-PPh ₂) ₂ (μ-dppf) (2)			
Au–Mn(1)	2.660(1)	Au–Mn(2)	2.776(1)
Mn(1)–Mn(2)	3.049(2)	Au–P(1)	2.318(2)
Mn(1)–P(2)	2.280(2)	Mn(2)–P(2)	2.285(2)
Mn(1)–C(1)	1.78(1)	Mn(1)–C(2)	1.829(9)
Mn(1)–C(3)	1.829(9)	Mn(1)–C(4)	1.83(1)
Mn(2)–C(5)	1.787(8)	Mn(2)–C(6)	1.841(8)
Mn(2)–C(7)	1.842(8)	Mn(2)–C(8)	1.850(8)
mean Fe–C	2.049(7)	mean C–O(1–4)	1.15(1)
mean C–O(5–8)	1.14(1)		
Mn(1)–Au–Mn(2)	68.20(3)	Au–Mn(1)–Mn(2)	57.71(3)
Au–Mn(2)–Mn(1)	54.09(3)	Mn(1)–P(2)–Mn(2)	83.82(7)
Mn(1)–Mn(2)–P(2)	48.02(6)	Mn(2)–Mn(1)–P(2)	48.16(6)
Mn(1)–Au–P(1)	149.43(5)	Mn(2)–Au–P(1)	142.34(5)
Au–Mn(1)–P(2)	104.86(6)	Au–Mn(2)–P(2)	101.17(6)
Au–Mn(1)–C(1)	161.7(3)	Au–Mn(1)–C(2)	71.3(3)
Au–Mn(1)–C(3)	81.0(2)	Au–Mn(1)–C(4)	90.5(3)
Au–Mn(2)–C(5)	155.2(3)	Au–Mn(2)–C(6)	68.2(2)
Au–Mn(2)–C(7)	75.1(2)	Au–Mn(2)–C(8)	105.8(3)
Mn(1)–C(1)–O(1)	176.8(9)	Mn(1)–C(2)–O(2)	170.9(8)
Mn(1)–C(3)–O(3)	178.9(7)	Mn(1)–C(4)–O(4)	177.5(8)
Mn(2)–C(5)–O(5)	177.1(7)	Mn(2)–C(6)–O(6)	172.4(6)
Mn(2)–C(7)–O(7)	175.5(6)	Mn(2)–C(8)–O(8)	173.4(8)
C(3)–Mn(1)···Mn(2)–C(7)	7.5(3)	C(3)–Mn(1)···Mn(2)–C(8)	–172.1(4)
C(4)–Mn(1)···Mn(2)–C(7)	–166.0(4)	C(4)–Mn(1)···Mn(2)–C(8)	14.5(4)
(b) PPN[Au{Mn ₂ (CO) ₈ (μ-PPh ₂) ₂] (7)			
Au–Mn(1)	2.800(1)	Au–Mn(1)a	2.780(1)
Au–Mn(2)	2.812(1)	Au–Mn(2)a	2.812(1)
Mn(1)···Mn(2)	3.105(2)	Mn(1)–P(1)	2.279(2)
Mn(2)–P(1)	2.275(2)	Mn(1)–C(1)	1.842(8)
Mn(1)–C(2)	1.766(8)	Mn(1)–C(3)	1.852(8)
Mn(1)–C(4)	1.801(8)	Mn(2)–C(5)	1.770(7)
Mn(2)–C(6)	1.850(8)	Mn(2)–C(7)	1.865(8)
Mn(2)–C(8)	1.828(8)	C(1)–O(1)	1.13(1)
C(2)–O(2)	1.16(1)	C(3)–O(3)	1.14(1)
C(4)–O(4)	1.17(1)	C(5)–O(5)	1.157(9)
C(6)–O(6)	1.14(1)	C(7)–O(7)	1.13(1)
C(8)–O(8)	1.144(9)	N–P(2)	1.596(3)
N–P(2)a	1.596(3)	Mn(1)···Mn(1)a	5.143(2)
Mn(1)···Mn(2)a	5.200(2)	Mn(2)···Mn(2)a	5.111(2)
Mn(1)–Au–Mn(2)	67.19(3)	Mn(1)–Au–Mn(1)a	133.42(4)
Mn(1)–Au–Mn(2)a	135.85(3)	Mn(2)–Au–Mn(2)a	130.70(4)
Au–Mn(1)–P(1)	103.51(6)	Au–Mn(2)–P(1)	103.26(6)
Mn(1)–P(1)–Mn(2)	85.99(7)	Au–Mn(1)–C(1)	95.9(2)
Au–Mn(1)–C(2)	161.6(2)	Au–Mn(1)–C(3)	79.6(2)
Au–Mn(1)–C(4)	69.6(2)	Au–Mn(2)–C(5)	160.1(2)
Au–Mn(2)–C(6)	97.9(2)	Au–Mn(2)–C(7)	79.1(2)
Au–Mn(2)–C(8)	68.9(2)	P(1)–Mn(1)–C(1)	86.6(2)
P(1)–Mn(1)–C(2)	93.2(2)	P(1)–Mn(1)–C(3)	94.5(2)
P(1)–Mn(1)–C(4)	170.2(3)	P(1)–Mn(2)–C(5)	94.6(2)
P(1)–Mn(2)–C(6)	85.3(2)	P(1)–Mn(2)–C(7)	95.3(2)
P(1)–Mn(2)–C(8)	168.0(2)	C(1)–Mn(1)–C(3)	175.5(3)
C(6)–Mn(2)–C(7)	177.0(3)	Mn(1)–C(1)–O(1)	175.8(7)
Mn(1)–C(2)–O(2)	177.7(7)	Mn(2)–C(3)–O(3)	175.7(6)
Mn(1)–C(4)–O(4)	169.7(6)	Mn(2)–C(5)–O(5)	178.4(6)
Mn(2)–C(6)–O(6)	175.2(6)	Mn(2)–C(7)–O(7)	175.0(6)
Mn(2)–C(8)–O(8)	169.0(6)		
C(1)–Mn(1)···Mn(2)–C(6)	165.7(3)	C(1)–Mn(1)···Mn(2)–C(7)	–16.7(3)
C(3)–Mn(1)···Mn(2)–C(6)	–18.2(3)	C(3)–Mn(1)···Mn(2)–C(7)	159.4(3)

stronger σ donor. On the other hand, **4** shows no activity toward free dppf at room temperature.

Since the two AuMn₂ triangles are not expected to communicate when separated by a phosphine bridge, a natural question one would ask is “Could we remove the bridge and fuse the triangles?”. The observed lability of P(OEt)₃ in **5** prompted us to use AuCl(SMe₂) as a source of “naked” gold which would achieve this fusion. Although a similar reaction of AuCl(SMe₂) with [Mn(CO)₅][–] did not give the expected linear cluster [(OC)₅Mn–Au–Mn(CO)₅][–]²¹ but significant decomposition instead,²² the use of a dimanganese monoanion, *i.e.*

1, as a precursor not only should allow a higher nuclearity cluster to form but also should stabilize the product, as there is less electron charge on the gold center as a result of its higher formal oxidation state (+1). The spectroscopic data (IR and ¹H and ³¹P NMR) suggested the formation of the expected anionic cluster PPN[Au{Mn₂(CO)₈(μ-PPh₂)₂] (7) (Scheme 1). An X-ray crystallographic study revealed four pseudo-octahedral [Mn(CO)₄] moieties fused at a gold center, which has a

(21) Braunstein, P.; Dehand, J. *J. Organomet. Chem.* **1975**, *88*, C24.
 Braunstein, P.; Schubert, U.; Burgard, M. *Inorg. Chem.* **1984**, *23*, 4057.
 (22) Low, P. M. N. and Hor, T. S. A. Unpublished results.

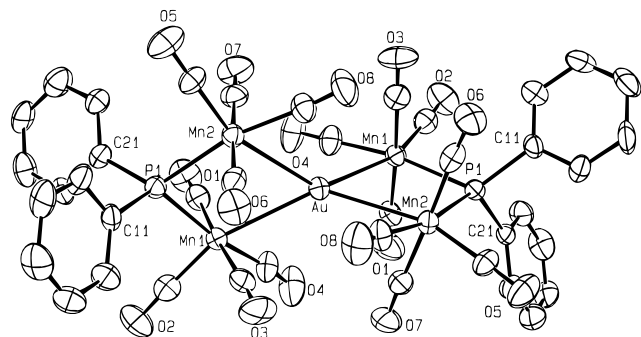


Figure 2. ORTEP drawing of the anion of $\text{PPN}[\text{Au}\{\text{Mn}_2(\text{CO})_8(\mu\text{-PPh}_2)\}_2]$ (**7**).

crystallographic C_2 symmetry, giving a bowtie configuration of the metals in the cluster (Figure 2). A similar configuration was proposed for the isoelectronic $\text{Hg}[\text{Mn}_2(\text{CO})_8(\mu\text{-PPh}_2)]_2$ although its crystallographic structure has not been established.²³ This bowtie is twisted with two AuMn_2P planes (maximum deviation 0.04 Å) fused at an angle of $85.50(4)^\circ$. The *endo* $\angle\text{Mn}(1)\text{-Au-Mn}(2)$ angle ($67.19(3)^\circ$) is significantly smaller than the tetrahedral angle, whereas the *exo* $\angle\text{Mn}(1)\text{-Au-Mn}(2a)$ and ($135.85(3)^\circ$) is significantly larger. This distortion of Au from an ideal tetrahedral geometry is required for its participation in a $\{\text{PMn}_2\text{Au}\}$ ring system. The Mn atoms are also highly distorted from an ideal octahedron; e.g., the $\text{Au-Mn}(1)$ vector is tilted away from the normal of the plane defined by $\text{Mn}(1)\text{-P}(1)\text{-C}(1)\text{-C}(3)\text{-C}(4)$ and the axial COs ($\text{C}(1,3/6,7)\text{-O}(1,3/6,7)$) are twisted at *ca.* $17.5(3)^\circ$ from parallel. The latter distortion is less severe in **2** (*ca.* $11.0(4)^\circ$). A carbonyl on each Mn group is bent ($\angle\text{Mn}(1)\text{-C}(4)\text{-O}(4) = 169.7(6)^\circ$ and $\angle\text{Mn}(2)\text{-C}(8)\text{-O}(8) = 169.0(6)^\circ$) in order to avoid nonbonding contacts between the two metallacyclic planes. The PPh_2 group symmetrically bridges the two Mn centers ($\text{Mn-P} = 2.279(2), 2.275(2)$ Å). As expected, without the influence of *dppf* as in **2**, the bite of gold on the phosphido-bridged Mn atoms is essentially symmetrical ($\Delta(\text{Au-Mn}) = 0.012(1)$ Å).

An important question on the structures of **2** and **7** is the strength of the Mn-Mn bonds compared to those in **1**, $\text{Mn}_2(\text{CO})_8(\mu\text{-H})(\mu\text{-PPh}_2)$, and $(\text{PR}_3)\text{AuMn}_2(\text{CO})_8(\mu\text{-PPh}_2)$ and the Au-Mn bonds compared to those in $(\text{PR}_3)\text{AuMn}_2(\text{CO})_8(\mu\text{-PPh}_2)$ and other Au-Mn clusters and whether these bonds are anticipated from the EAN rule or other bonding theories. The Mn-Mn distance in complex **2** ($3.049(2)$ Å) seems without doubt to indicate direct Mn-Mn bonding when compared to other Mn-Mn-bonded systems²⁴ (e.g. Mn-Mn in $\text{Mn}_2(\text{CO})_{10}$ is $2.9038(6)$ Å²⁵). It is very similar to those found in $(\text{PPhR}_2)\text{AuMn}_2(\text{CO})_8(\mu\text{-PPh}_2)$ ($\text{R} = \text{Ph}$ ($3.067(3)$ Å),¹³ Me ($3.066(8)$ Å)¹⁴). The EAN rule supports the Mn-Mn bond formation on the basis of the one-electron contribution from $\text{Au}(\text{PPhR}_2)$ as its isolobal counterpart H. It is, however, significantly longer, and presumably weaker, than that in $\text{Mn}_2(\text{CO})_8(\mu\text{-H})(\mu\text{-PPh}_2)$ ($2.951(1)$ ¹⁴ and $2.937(5)$ Å²⁶), which in turn is

significantly weaker than that in **1** ($2.867(2)$ Å).¹⁴ This bond lengthening upon protonation and auration is generally explained on geometric and electronic grounds.¹⁴ The Au-Mn bonds (mean $2.718(1)$ Å) appear to be consistent with those in AuMn_2 ($2.68\text{--}2.84$ Å) and higher nuclearity clusters, e.g. $\{(\text{PPh}_3)\text{Au}\}_4\text{Mn}(\text{CO})_5\text{-BF}_4$ ($2.658(4)\text{--}2.766(5)$ Å),¹⁵ $\text{PPh}_3\text{AuMn}_2(\text{CO})_8(\mu\text{-PPh}_2)$ ($2.678(3)\text{--}2.710(3)$ Å),¹³ $\{(\text{PPh}_3)\text{Au}\}_2\text{Mn}_2(\text{CO})_6(\mu\text{-C}(\text{Ph})\text{O})(\mu\text{-PPh}_2)$ ($2.702(2)\text{--}3.084(2)$ Å),¹³ $\{(\text{PPh}_3)\text{Au}\}_2\text{Mn}_2(\text{CO})_8(\mu\text{-PCy})$ ($2.762(2)$ Å),²⁷ $\text{Mn}_2(\mu\text{-AuPCy}_3)(\mu\text{-PCy}_3)(\text{CO})_8$ ($2.688(1)\text{--}2.726(1)$ Å),²⁷ and $\{(\text{PPh}_3)\text{Au}\}_3\text{-Mn}_2(\text{CO})_6(\mu\text{-PPh}_2)\cdot\text{CH}_2\text{Cl}_2$ ($2.698(2)\text{--}2.742(3)$ Å).¹³ All these Au-Mn bonds are longer than those in the bimetallic system (e.g. $\text{PPh}_3\text{Au-Mn}(\text{CO})_5$ ($2.52(3)$ Å)²⁸ and $\text{PPh}_3\text{Au-Mn}(\text{CO})_4\{\text{P}(\text{O}i\text{Pr})_3\}$ ($2.57(1)$ Å).²⁹

For **7**, both the phosphido-bridged Mn-Mn ($3.105(2)$ Å) and Au-Mn (mean $2.806(1)$ Å) lengths are significantly longer than those of their counterparts in **2**. The Mn-Mn length is longer than all the Mn-Mn bonds found in the known AuMn_2 trinuclear species ($2.748\text{--}3.080$ Å; mean 2.926 Å).^{13-15,27,30,31} These unexpectedly long M-M distances in **7** compared to those in **1** and **2** raised a number of questions regarding the M-M bonds; two important issues are "Are there Mn-Mn bonds in **7**?" and "Why are the Mn-Mn and Au-Mn bonds weaker in **7** compared to **2**?"

The opening up of $\angle\text{Mn-P-Mn}$ from **2** ($83.82(7)^\circ$) to **7** ($85.99(7)^\circ$) despite the statistically identical Mn-P bonds in these molecules ($2.282(2)$ Å in **2** and $2.277(2)$ Å in **7**) appears to suggest some repulsive forces between the Mn atoms in **7**. However, the Mn-Mn bond in **7** is only $0.056(2)$ Å longer than that found in **2** and Mn-Mn σ bonds have been reported to be as long as 3.23 Å.²⁴ The bond length found in the crystal structure therefore does not provide a conclusive answer to whether there are direct Mn-Mn bonds in **7**. The EAN rule provides a guide but not necessarily an answer.³² Complex **7**, being a 78-electron cluster, would require six M-M bonds if all five metal atoms are in adherence with the 18-electron configuration (e.g. $\text{Os}_5(\text{CO})_{19}$ ³³). This is, however, unlikely for gold³⁴ and is not consistent with the observed structure. On the basis of a simple localized orbital approach assuming 18-electron Mn, one could propose the presence of 5 (**I**), 4 (**II**), or even 3 (**III**) M-M bonds based on 16-, 14- and 12-electron configurations, respectively, for gold. In each of these, a series

(27) Haupt, H.-J.; Schwefler, M.; Flörke, U. *Inorg. Chem.* **1995**, *34*, 292.

(28) Powell, H. M.; Mannan, K.; Kilbourn, B. T.; Porta, P. *Proc. Int. Conf. Coord. Chem.* **1964**, *8*, p 155.

(29) Mannan, Kh. A. I. F. M. *Acta Crystallogr.* **1967**, *23*, 649.

(30) Riera, V.; Ruiz, M. A.; Tiripichio, A.; Camellini, M. T. *J. Chem. Soc., Dalton Trans.* **1987**, 1551. Carreño, R.; Riera, V.; Ruiz, M. A.; Bais, C.; Jeannin, Y. *Organometallics* **1992**, *11*, 2923.

(31) The only other AuMn_4 bowtie cluster known is $\text{AuMn}_4(\text{CO})_{12}(\mu\text{-tedip})_2(\mu\text{-H})_5$ (*tedip* = $(\text{EtO})_2\text{POP}(\text{OEt})_2$), which is a 76-electron cluster with Mn-Mn = $2.860(2)$ and $3.080(2)$ Å and mean Au-Mn = $2.822(2)$ Å (see: Carreño, R.; Riera, V.; Ruiz, M. A.; Tiripichio, A.; Tiripichio-Camellini, M. *Organometallics*, **1994**, *13*, 993). It, however, cannot be compared directly with complex **7** because the bridging ligands are entirely different and the electronic saturations are not the same.

(32) Bernal *et al.* have drawn a similar conclusion after studying the Mn-Mn distances of a series of dimanganese complexes. The authors found an unpredictably wide range of Mn-Mn lengths, which led them to conclude that there is "a need for caution in using simple rules (such as the EAN rule) to explain metal-metal distances". Refer to: Creswick, M.; Bernal, I.; Reiter, B.; Herrmann, W. A. *Inorg. Chem.* **1982**, *21*, 645.

(33) Farrar, D. H.; Nicholls, J. N.; Jackson, P. F.; Johnson, B. F. G.; Lewis, J. *J. Chem. Soc., Chem. Commun.* **1981**, 273. Nicholls, J. N. *J. Chem. Soc., Dalton Trans.* **1982**, 1395.

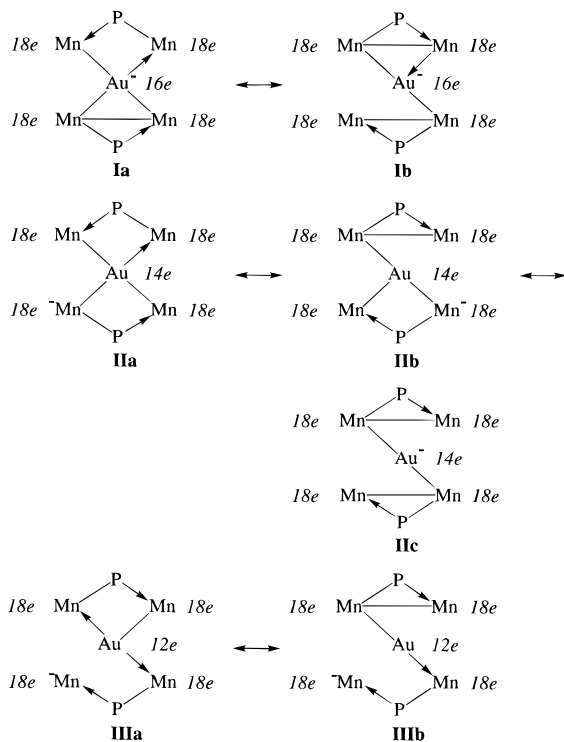
(34) Hall, K. P.; Mingos, D. M. P. *Prog. Inorg. Chem.* **1984**, *32*, 237.

(23) Iggo, J. A.; Mays, M. J. *J. Chem. Soc., Dalton Trans.* **1984**, 643.

(24) Bernal, I.; Creswick, M.; Herrmann, W. A. *Z. Naturforsch., B: Anorg. Chem., Org. Chem.* **1979**, *B34*, 1345.

(25) Churchill, M. R.; Amoh, K. N.; Wasserman, H. J. *Inorg. Chem.* **1981**, *20*, 1609.

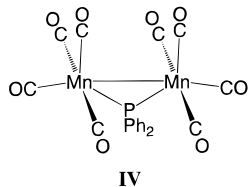
(26) Doedens, R. J.; Robinson, W. T.; Ibers, J. A. *J. Am. Chem. Soc.* **1967**, *89*, 4323.



of "no-bond" resonance structures (I–III) can then be constructed which explain the weakness of both Mn–Mn and Au–Mn bonds. In this bowtie arrangement, all four Mn atoms are interconnected through the Au center; electron delocalization thus helps to stabilize the two metal planes and keep the cluster intact. These localized-bond concepts can give a qualitative idea of the M–M bonds but could not illustrate the nature and relative importance of the metal orbitals in these bonds.

As an attempt to address such issues, Fenske–Hall molecular orbital calculations were carried out on models of **1**, **2**, **7**, $\text{Mn}_2(\text{CO})_8(\mu\text{-H})(\mu\text{-PPh}_2)$ (**8**), and $(\text{PMe}_2\text{-Ph})\text{AuMn}_2(\text{CO})_8(\mu\text{-PPh}_2)$ (**9**). For comparison, their Mn–Mn distances are 2.867(2), 3.049(2), 3.105(2), 2.951(1), and 3.066(8) Å, respectively. For simplicity, let the Mn–Mn line be along the z axis, so that the d_z^2 orbitals are directed at one another.

Upon inspection of the structures of the compounds, it is readily apparent that in the anion **1**,¹⁴ the Mn–Mn bond is a component of the σ -bonding framework (IV). In the other compounds, the orientation of the



Mn–C bonds with respect to the Mn–Mn and Mn–Au/H bonds³⁵ indicates that the latter constitutes the sixth bond in the Mn pseudo-octahedron;¹⁴ it can thus be inferred that Mn–Au/H interactions are dominant over Mn–Mn interactions. This is reflected in the total

(35) In $[\text{Mn}_2(\text{CO})_8(\mu\text{-PPh}_2)]^-$, the molecular planes containing the metals and phosphorus have two carbonyls at approximately right angles (and another two *trans*) to the Mn–Mn bond. In both **2** and **7**, these carbonyls move away from the Mn–Mn axis so as to accommodate the bridging gold atom. As a result, these carbonyls are *trans* to phosphorus and the sites opposite the Mn–Mn axis are vacant.

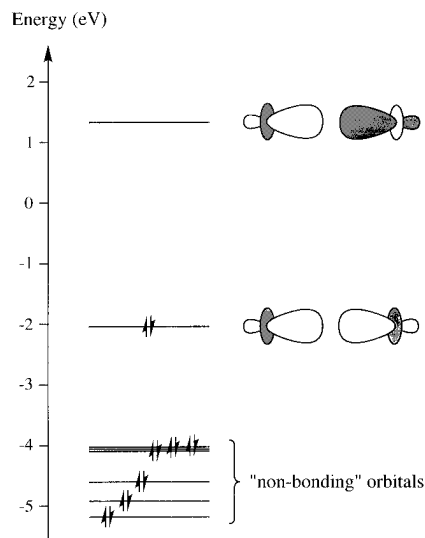


Figure 3. Energy levels of the filled Mn-based molecular orbitals in **1**. The HOMO is Mn–Mn σ bonding, while the LUMO is antibonding.

Table 3. Calculated Total Overlap Populations and Mn–Mn d_z^2 – d_z^2 and Mn d_z^2 –Au/H (all orbitals) Partial Overlap Populations for Mn–Mn and Mn–Au/H Interactions in Models of Compounds **1, **2**, **7**, **8**, and **9****

compd	overlap pop.	Mn–Mn	Mn(1)–Au/H	Mn(2)–Au/H
1	total	0.00127		
	d_z^2	0.0142		
2	total	–0.0091	0.0899	0.0559
	d_z^2	0.0078	0.0060	0.0040
7	total	–0.0142	0.0500	0.0461
	d_z^2	0.0044	0.0016	0.0016
8	total	–0.0177	0.1078	0.1073
	d_z^2	0.0055	0.0294	0.0293
9	total	–0.0084	0.0727	0.0862
	d_z^2	0.0079	0.0050	0.0051

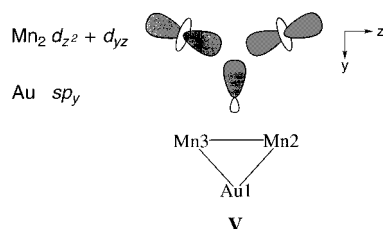
Mn–Mn, Au–Mn, and Mn–H overlap populations in these compounds (Table 3). With regard to Mn–Mn interactions, it is striking to observe that only in the case of **1** is the overlap population positive; the rest are all negative.

From a qualitative viewpoint, accounting for all the electrons necessitates the filling of three "nonbonding" orbitals³⁶ per Mn, leaving two electrons (four for compound **7**) for Mn–Mn/Au/H interactions. In **1** the d_z^2 orbitals do not belong to the nonbonding set; their interaction yields a bonding and an antibonding orbital, and the two electrons available for Mn–Mn interaction fill the bonding orbital (Figure 3).³⁷ On the other hand, in **2**, **7**, **8**, and **9**, Mn–Mn is not a dominant σ interaction; therefore, the d_z^2 orbitals are part of the nonbonding set. Under normal circumstances one would expect filled d_z^2 bonding and antibonding orbitals, resulting in a net antibonding interaction.

We focus on the electronic structure of **9** as a prototype of the compounds with Au or H. The HOMO describes a two-electron–three-center bond (as described by Hall and Mingos³⁴) involving Au and the two Mn atoms (V). It is interesting to note that the Mn–Mn d_z^2 combinations mix with the Mn d_{yz} and Au

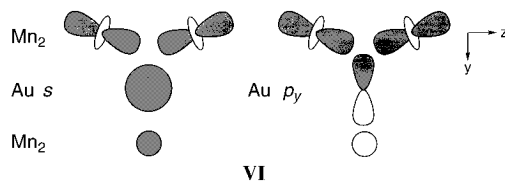
(36) These orbitals participate in π interactions. It should be noted in **1** that this set has σ -antibonding contributions due to severe distortion from a perfect octahedron.

(37) Contributions to the seven filled Mn-based MO's as well as the LUMO are given as Supporting Information.



orbitals: the bonding combination occurs in the HOMO6, HOMO5, and HOMO, while the antibonding combination occurs in the HOMO2 and LUMO. The major contributions to the HOMO2, HOMO, and LUMO are listed in Table 4.³⁸ (Note that Mn d_{yz} is involved in a σ interaction with Au.) Despite its presence in the HOMO, Mn d_z^2 does not play a major role in Mn–Au bonding, as can be inferred from the partial d_z^2 –Au overlap populations listed in Table 3. From considerations of “orbital conservation”, it can be inferred that mixing allows the antibonding combination to be partially unoccupied (as part of the LUMO), and thus results in a weak d_z^2 bonding interaction, as shown by their partial overlap populations (Table 3). This allows the two Mn atoms to approach each other more closely, even though the total overlap population is negative.³⁹

As described by the HOMO (Table 4), in **9** Au interacts with the Mn_2 moiety mainly through a hybrid of its s and p_y orbitals (V; the same is true of **2**). In contrast, of the two MO's in **7** which are the counterparts of the HOMO in **9**, one utilizes only the Au s orbital and the other only the p_y orbital (shown qualitatively in VI); since Au is situated on a symmetry axis,



all the MO's must be either symmetric or antisymmetric with respect to Au, thus precluding sp mixing. Consequently, there is no Au orbital reinforcement in the direction of any Mn_2 moiety. This is a likely cause for weaker Au–Mn interactions, as reflected in the longer Au–Mn bond lengths.

With regard to the longer Mn–Mn distance in **7**, the same symmetry constraints apply to the mixing of Mn “ d_z^2 ”-type⁴⁰ orbitals with Au orbitals. However, the dominance of the Au–Mn interactions and the foregoing results suggest that the length of the Mn–Mn bond is largely determined by the strength of the Au–Mn interactions, especially since the latter involve mainly the Au s and p_y orbitals. This conclusion can be generalized to include compounds **2**, **8** (Mn–H), and **9**; in **8** the size of H could also be important.

The interaction described by HOMO2 of **9** deserves some comment. This is actually Au–Mn antibonding (with mixing to minimize the “bad” interaction), but there are corresponding lower energy bonding molecular orbitals involving Au d_{yz} and Mn σ orbitals. The Au d_{yz}

Table 4. Major Orbital Contributions to the HOMO2, HOMO, and LUMO of **9^a**

atomic orbital	HOMO2	HOMO	LUMO
Au			
d_{yz}	0.1461	0.0662	0.0397
s	0.0235	−0.3342	−0.0495
p_y	−0.0344	0.2623	0.0268
p_z	0.2111	−0.0085	−0.3352
Mn2			
d_z^2	−0.5116	−0.2452	−0.4338
d_{yz}	−0.2841	0.1888	0.1003
Mn3			
d_z^2	0.2243	−0.3841	0.4046
d_{yz}	−0.2238	−0.1596	0.0678

^a See V for relative positions of atoms. The energies of these molecular orbitals are −8.04, −6.97, and −4.41 eV, respectively.

interaction, which accounts for an average of 14% of the total Au–Mn overlap populations in **9**, is present in all the compounds with Au. In a sense, it could be considered as π back-donation from the filled Au d_{yz} orbital into the Mn σ orbitals, somewhat analogous to the behavior of Au toward phosphine ligands.

The isolobal principle prompted some intensive work on $[AuPR_3]^+$ and H^+ in edge-bridging a variety of M–M-bonded anions.^{6a–c,8,34,41,42} This study showed that, by stripping off the phosphine, one can have a direct access to a bowtie cluster. The strength of the homo and hetero metal–metal bonds appears to be dependent not only on the electronic state of the metals but also on their ligand arrangements. Future directions of our project are charted by these findings.

Experimental Section

General Procedures. All reactions were performed under pure dry argon using standard Schlenk techniques. $Mn_2(CO)_8(\mu-H)(\mu-PPh_2)^{17}$ and $PPN[Mn(CO)_8(\mu-PPh_2)]^{14}$ were prepared by literature methods. $Au_2Cl_2(\mu-dppf)^{43}$ was prepared by a modified procedure from $AuCl(SMe)^{44}$ and $dppf$ ⁴⁵ in a 2:1 molar ratio. $Au_2Cl_2(\mu-dppe)$ was prepared from $HAuCl_4$ and $dppe$ in a 1:3 ratio. All other reagents were commercial products and were used as received. FT-IR spectra were recorded on a Perkin-Elmer 1710 spectrometer. All NMR spectra were recorded in $CDCl_3$ solution on a Bruker AC 300F spectrometer. The ³¹P NMR chemical shifts are externally referenced to 85% H_3PO_4 . Elemental analyses were performed by the analytical service of this department. The presence of solvate molecules in the sample was confirmed by NMR analysis. The solvent inclusion in the crystal lattice of many $dppf$ complexes has been noted in the literature.⁴⁶ Molecular weight determination was carried out by vapor-pressure osmometry in a Knauer-Dampfdruck osmometer by Galbraith Laboratories, Inc., in Knoxville, TN, using toluene as solvent.

The models of the molecules used for the calculations are based on their crystal structures (see ref 14 and this work). All the phenyl rings and methyl groups on phosphine ligands were replaced by hydrogen atoms, and the P–H bond lengths

(41) Ferrer, M.; Reina, R.; Rossell, O.; Seco, M.; Alvarez, S.; Ruiz, E. *Organometallics* **1992**, *11*, 3753. Reina, R.; Rossell, O.; Seco, M.; Ros, J.; Yáñez, R.; Perales, A. *Inorg. Chem.* **1991**, *30*, 3973. Low, A. A.; Lauher, J. W. *Inorg. Chem.* **1987**, *26*, 3863.

(42) Hor, T. S. A.; Tan, A. L. C. *J. Coord. Chem.* **1989**, *20*, 311.

(43) Hill, D. T.; Girard, G. R.; McCabe, F. L.; Johnson, R. K.; Stupik, P. D.; Zhang, J. H.; Reiff, W. H.; Eggleston, D. S. *Inorg. Chem.* **1989**, *28*, 3529.

(44) Bonati, F.; Minghetti, G. *Gazz. Chim. Ital.* **1973**, *103*, 373.

(45) Marr, G.; Hunt, T. *J. Chem. Soc. C* **1969**, 1070. Bishop, J. J.; Davison, A.; Katcher, M. L.; Lichtenberg, D. W.; Merrill, R. E.; Smart, J. C. *J. Organomet. Chem.* **1971**, *27*, 241.

(46) Butler, I. R.; Cullen, W. R.; Kim, T. J.; Rettig, S. J.; Trotter, J. *Organometallics* **1985**, *4*, 972.

(38) Contributions to all filled Au/Mn-based orbitals as well as the LUMO of **9** are given as Supporting Information.

(39) The overall negative overlap population is due to net antibonding π interactions.

(40) Only one Mn–Mn line can be parallel to the z axis.

were adjusted to the sum of covalent radii. The models were aligned such that one Mn–Mn line is parallel to the *z* axis and the Mn–Au–Mn plane is parallel to the *yz* plane. In **9**, the bridging hydride, whose coordinates were not given in the crystal structure, was placed in the same plane as the Mn–P–Mn triangle, with Mn–H distances slightly longer than the sum of covalent radii.

Calculations were performed using the self-consistent Fenske–Hall approximate molecular orbital method.⁴⁷ Except for hydrogen, the basis functions were obtained by fitting the results of $X\alpha$ (Herman–Skillman) calculations⁴⁸ for M(+1) (transition metals) and X(0) (main-group metals) to Slater orbitals.⁴⁹ Double- ζ functions were used for transition-metal valence d orbitals and main-group valence p orbitals; all the rest were single- ζ functions. An orbital exponent of 1.2 was used for hydrogen.

Reaction of PPN[Mn₂(*u*-PPh₂)(CO)₈] (1) with Au₂Cl₂(*u*-dppf). A solution of AgBF₄ (0.050 g, 0.26 mmol) in thf (5 cm³) was added to that of Au₂Cl₂(*u*-dppf) (0.101 g, 0.098 mmol), which led to an immediate precipitation of AgCl. The solution, shielded from direct light, was stirred for *ca.* 1 h before filtering dropwise into a flask containing a yellow solution of PPN-[Mn₂(CO)₈(*u*-PPh₂)] (**1**; 0.100 g, 0.095 mmol) in CH₂Cl₂ (5 cm³). The resultant orange-red mixture was further stirred at room temperature for *ca.* 3 h. The solvent was removed and the orange-red residue obtained redissolved in a minimum amount of CH₂Cl₂ and chromatographed on silica TLC plates. Elution with CH₂Cl₂/hexane (2:5) gave two major bands, which were extracted with CH₂Cl₂ and recrystallized from a CH₂Cl₂/hexane mixture to give, in order of decreasing *R_f* value, [AuMn₂(CO)₈(*u*-PPh₂)₂(*u*-dppf)] (**2**; 0.050 g, 51%) and AuCl(*u*-dppf)[AuMn₂(CO)₈(*u*-PPh₂)] (**3**; 0.020 g, 13%). A third minor band near the base line corresponds to unreacted Au₂Cl₂(*u*-dppf). Omitting AgBF₄ in a subsequent reaction and reversing the addition of **1** to Au₂Cl₂(*u*-dppf) (1:1) gave **2** in 50% yield but **3** in 20% yield. Anal. Calcd for **2**: C, 44.74; H, 2.43; Au, 19.83; Fe, 2.81; Mn, 11.06; P, 6.23. Found: C, 44.37; H, 2.38; Au, 17.41; Fe, 2.54; Mn, 10.03; P, 6.34. ¹H NMR (δ): 4.22 (q, CpH _{α} , 4H); 4.74 (m, CpH _{β} , 4H); 7.32–7.46 (m, Ph, 32H); 7.81–7.88 (m, Ph, 8H). ³¹P NMR (δ): 58.02 (s, P_{Au}); 212.31 (s, br, P_{Mn}). IR (CO, cm⁻¹): 2021 s, 1983 vs, 1956 s, 1930 s (CHCl₃). Mol wt (toluene): 2058, calcd 1987. Anal. Calcd for **3**: C, 43.16; H, 2.55; Au, 26.21; Cl, 2.36; Fe, 3.72; Mn, 7.31; P, 6.18. Found: C, 43.26; H, 2.76; Au, 25.52; Cl, 2.32; Fe, 3.45; Mn, 6.93; P, 6.28. ¹H NMR (δ): 4.22 (m, CpH _{α} (Au–Mn₂), 2H); 4.20 (m, CpH _{α} (Au), 2H); 4.72 (m, CpH _{β} , 4H); 7.33–7.54 (m, Ph, 26H); 7.82–7.88 (m, Ph_{PPH₂}, 4H). ³¹P NMR (δ): 27.82 (s, FcP_{AuCl}); 58.04 (s, FcP_{AuMn₂}); 212.31 (s, br, PPh₂). IR (CO, cm⁻¹): 2022 s, 1983 vs, 1957 s, 1930 s (CHCl₃). A 2:1 stoichiometric ratio of **1** to Au₂Cl₂(*u*-dppf) in the presence of AgBF₄ gave **2** in 65% yield but a negligible amount of **3**.

Reaction of Complex 1 with Au₂Cl₂(*u*-dppe). A solution of **1** (0.109 g, 0.103 mmol) in thf (25 cm³) was transferred dropwise to a solution of Au₂Cl₂(*u*-dppe) (0.109 g, 0.126 mmol) in CH₂Cl₂ (25 cm³). The mixture, which turned from colorless to orange, was stirred at room temperature for *ca.* 3 h and stripped of solvent and the orange residue was redissolved in a minimum amount of CH₂Cl₂. Development on silica TLC plates with CH₂Cl₂/hexane (2:5) gave [AuMn₂(*u*-PPh₂)(CO)₈]₂(*u*-dppe) (**4**; 0.026 g, 12%). Anal. Calcd for **4**: C, 43.31; H, 2.42; Au, 21.52; Mn, 12.06; P, 6.77. Found: C, 43.12; H, 2.45; Au, 20.15; Mn, 10.93; P, 7.26. ¹H NMR (δ): 2.97 (s, CH₂, 4H); 7.29–7.36 (m, Ph, 12H); 7.41–7.48 (m, Ph, 12H); 7.53–7.57 (m, Ph, 8H); 7.82–7.85 (m, Ph, 8H). ³¹P NMR (δ): 62.63 (s, P_{Au}); 215.46 (s, br, PPh₂).

Reaction of Complex 2 with PPh₃. A solution of **2** (0.065 g, 0.033 mmol) and PPh₃ (0.020 g, 0.076 mmol) in thf (25 cm³)

was refluxed for *ca.* 4 h. The reaction, followed by TLC, was stopped when there were no further changes on the TLC plates. The solvent was removed *in vacuo* and the orange residue extracted with ether to give an orange-red solution. Applying the ether extract to silica TLC plates and eluting with CH₂Cl₂/hexane (1:4) gave two products corresponding to, in order of decreasing *R_f* value, (PPh₃)AuMn₂(CO)₈(*u*-PPh₂) (**5**; 0.020 g, 31%) and unreacted **2** (0.008 g, 12%). Anal. Calcd for **5**: C, 44.74; H, 2.43; Au, 19.83; Fe, 2.81; Mn, 11.06; P, 6.23. Found: C, 44.35; H, 2.20; Au, 17.41; Fe, 2.52; Mn, 9.60; P, 6.30. ¹H NMR (δ): 7.28–7.36 (m, Ph, 5H); 7.44–7.60 (m, Ph, 16H); 7.82–7.88 (m, Ph, 4H). ³¹P NMR (δ): 63.01 (s, PPh₃); 212.54 (s, br, PPh₂). IR (CO, cm⁻¹): 2021 s, 1983 vs, 1955 s, 1930 s (CHCl₃).

Reaction of Complex 2 with P(OEt)₃. P(OEt)₃ (0.5 cm³, 2.92 mmol) was injected by a syringe into an orange solution of **2** (0.066 g, 0.033 mmol) in thf (8 cm³), which readily turned brownish yellow. The reaction was monitored by TLC. Two spots, in order of decreasing *R_f* value, corresponding to a major yellow product identified as (P(OEt)₃)AuMn₂(CO)₈(*u*-PPh₂) (**6**) and a minor compound identified as **2** were observed. After the mixture was stirred at room temperature for 2 h, the solvent was removed *in vacuo* and the residue extracted by a minimum amount of CH₂Cl₂ and chromatographed on silica TLC plates. Elution with CH₂Cl₂/hexane (1:1) and recrystallization with CH₂Cl₂/hexane gave band 1 as complex **6** (0.012 g, 21%) and band 2 as complex **2** (0.005 g, 8%). Anal. Calcd for **6**: C, 36.54; H, 3.18; Au, 21.78; Mn, 12.16; P, 6.85. Found: C, 36.14; H, 3.20; Au, 17.25; Mn, 9.57; P, 5.98. ¹H NMR (δ): 1.31 (t, CH₃, 9H, ³J_{HH} = 7.08 Hz); 4.13 (dq, CH₂, 6H, ³J_{HH} = 7.08 Hz, ³J_{PH} = 9.52 Hz); 7.19–7.27 (m, Ph, 6H); 7.64–7.89 (m, Ph, 4H). ³¹P NMR (δ): 182.67 (s, P(OEt)₃); 217.54 (s, br, PPh₂). IR (CO, cm⁻¹): 2029 s, 1985 vs, 1957 s, 1931 s (CHCl₃).

In the process of applying the mixture to the plates followed by elution, it was found that the relative intensities of the first (complex **6**) and second (complex **2**) bands changed with time. The earlier plates gave a higher proportion of **6** compared to **2**, while the later plates gave more **2** than **6**. This was the first indication that dppf replacement of **1** by P(OEt)₃ is reversible.

Reaction of Complex 1 with AuCl(SMe₂). A solution of **1** (0.155 g, 0.147 mmol) in thf (20 cm³) was cooled in an ice bath before it was transferred by a teflon delivery tube to a solution of AuCl(SMe₂) (0.038 g, 0.129 mmol) in dimethyl sulfide (2 cm³) at 0 °C to give an orange-red solution. The mixture was stirred in an ice bath for *ca.* 1/2 h followed by stirring at room temperature for *ca.* 4 h. The solvent was removed *in vacuo* and the dark brown residue washed with benzene (*ca.* 3 × 10 cm³) and then MeOH (2 × 10 cm³). The residue was extracted with acetone and filtered through celite to remove the fine Au particles. Hexane was added to the filtrate to give a red precipitate which was redissolved in CH₂Cl₂; hexane was then added. When this mixture stood for *ca.* 7 days, a red crystalline solid was isolated (at times, it may be necessary to remove some minor foreign crystals, which are orange-yellow, of **1**) to give orange-red crystals of PPN[Au{Mn₂(CO)₈(*u*-PPh₂)₂}]₂ (**7**; 0.025 g, 11%). The yield is low, as it is calculated on the basis of the amount of added AuCl(SMe₂), some of which inevitably decomposed in the course of reaction. Anal. Calcd for **7**: C, 51.46; H, 2.84; Au, 11.10; Mn, 12.38; N, 0.79; P, 6.98. Found: C, 51.41; H, 2.77; Au, 9.90; Mn, 11.77; N, 0.83; P, 6.89. ¹H NMR (δ): 7.35–7.89 (m, Ph, 50H). ³¹P NMR (δ): 22.54 (s, N(PPh₃)₂⁺); 190.71 (s, br, Mn–PPh₂). IR (CO, cm⁻¹): 2041 w, 2014 s, 1984 vs, 1971 m, sh, 1910 s, br (acetone).

Crystallographic Analysis. Red crystals of complexes **2** and **7** were grown at room temperature (25 °C) by a layering method, with hexane on a sample solution in CH₂Cl₂, and slow evaporation of a sample solution in a mixture of CH₂Cl₂ and hexane, respectively. Single crystals of dimensions 0.19 × 0.31 × 0.38 mm for **2** and 0.50 × 0.09 × 0.22 mm for **7** were chosen

(47) Hall, M. B.; Fenske, R. F. *Inorg. Chem.* **1972**, *11*, 768.

(48) Herman, F.; Skillman, S. *Atomic Structure Calculations*; Prentice-Hall: Englewood Cliffs, NJ, 1963.

(49) Bursten, B. E.; Jensen, J. R.; Fenske, R. F. *J. Chem. Phys.* **1978**, *68*, 3320.

for the X-ray diffraction study with graphite-monochromated Mo K α ($\lambda = 0.709\ 30\ \text{\AA}$ for **2** and $\lambda = 0.710\ 69\ \text{\AA}$ for **7**) radiation at room temperature. The crystal data and experimental conditions are given in Table 1. Atomic coordinates and equivalent isotropic displacement coefficients are given in the Supporting Information. The unit cell constants were determined by a least-squares fit to the setting parameters of 25 independent reflections in the range of $17.26^\circ < 2\theta < 36.08^\circ$ for **2** and $15.77^\circ < 2\theta < 62.48^\circ$ for **7**. Totals of 4611 for **2** ($2\theta_{\text{max}} = 44.8^\circ$) and 4642 unique reflections for **7** ($2\theta_{\text{max}} = 44.9^\circ$) were measured by scanning on a Nonius diffractometer. The range of indices was $h = -15$ to $+15$, $k = 0-15$, $l = 0-17$ for **2** and $h = -26$ to $+25$, $k = 0-18$, $l = 0-18$ for **7**. After corrections for absorption effects, 3462 data with $I > 3.0\sigma(I)$ were used for **2** and 3169 data with $I > 2.5\sigma(I)$ for **7**. The minimum and maximum transmission factors were 0.368 and 0.999 for **2** and 0.781 148 and 0.999 825 for **7**. The structures were solved by direct methods and MULTAN.⁵⁰ Refinement was by full-matrix least-squares calculations with all non-hydrogen atoms allowed anisotropic motion. All hydrogen atoms were fixed as isotropic ellipsoids in the final cycles of least-squares refinement. The last least-squares cycle was calculated with 75 atoms, 457 parameters, and 3462 reflections and converged with $R_F = 0.030$, $R' = 0.035$ (GOF 1.43) (for all reflections $R_F = 0.052$, $R' = 0.036$) for **2** and with 77 atoms, 461 parameters, and 3169 reflections and converged with $R_F = 0.031$, $R' = 0.033$ (GOF 1.10) (for all reflections $R_F = 0.063$, $R' = 0.038$) for **7**. Weights based on counting statistics were used. The weight modifier was 0.000 100. The maximum shift/error ratio was

(50) Main, P.; Fiske, S. E.; Hull, S. L.; Germain, G.; Declercq, J. P.; Woolfson, M. H. In MULTAN, a System of Computer Programs for Crystal Structure Determination from X-ray Diffraction Data; Universities of York and Louvain, 1980.

0.001 for **2** and 0.004 for **7**. In the last difference map the deepest hole was $-0.590\ \text{e}\ \text{\AA}^{-3}$ and the highest two peaks of 1.580 and $1.102\ \text{e}\ \text{\AA}^{-3}$ were at $1.11\ \text{\AA}$ from the gold atom in **2**. The next positive peak height was $<0.4\ \text{e}\ \text{\AA}^{-3}$. For **7**, the deepest hole and highest peak were -0.320 and $0.350\ \text{e}\ \text{\AA}^{-3}$. Computations were carried out on a microVAX 3600 computer with the NRCC package. Selected bond distances and angles are listed in Table 2. For **7**, both PPN^+ and $[\text{Au}\{\text{Mn}_2(\text{CO})_8(\mu\text{-PPh}_2)_2\}]^-$ are required to possess a rigorous C_2 molecular symmetry in the solid state because the central Au and N atoms are located on crystallographic 2-fold axes. Only half of the atoms in the formula are thus crystallographically independent.

Acknowledgment. Financial assistance from the National University of Singapore (NUS; Grant No. RP850030) and technical help from our department at NUS are gratefully acknowledged. We especially thank Y. L. Yong and S. L. Boo for experimental assistance and Y. P. Leong for stenographic work. A.L.T. would like to acknowledge the National Science and Technology Board for financial support through a Postdoctoral Fellowship.

Supporting Information Available: Tables giving crystal data and refinement details, positional and thermal parameters, bond distances and angles, and torsion angles for **2** and **7**, least-squares plane data for **7**, and MO data for **1** and **9** (26 pages). Ordering information is given on any current masthead page.

OM950797G